Chemical Science

ROYAL SOCIETY OF CHEMISTRY

EDGE ARTICLE

View Article Online
View Journal | View Issue

Cite this: *Chem. Sci.*, 2023, **14**, 4724

All publication charges for this article have been paid for by the Royal Society of Chemistry

Received 17th February 2023
Accepted 13th April 2023

DOI: 10.1039/d3sc00909b

rsc.li/chemical-science

On the existence of low-valent magnesium–calcium complexes†‡

Jonathan Mai, Bastian Rösch, Neha Patel, Jens Langer and Sjoerd Harder *

DFT-Calculations predict that a low-valent complex (BDI)Mg–Ca(BDI) with bulky β-diketiminate (BDI) ligands is thermodynamically stable. It was attempted to isolate such a complex by salt-metathesis between $[(^{DIPeP}BDI^*)Mg^-Na^+]_2$ and $[(^{DIPeP}BDI)CaI]_2$ ($^{DIPeP}BDI$ = HC[C(Me)N-DIPeP]$_2$; $^{DIPeP}BDI^*$ = HC[C(*t*Bu)N-DIPeP]$_2$; DIPeP = 2,6-CH(Et)$_2$-phenyl). Whereas in alkane solvents no reaction was observed, salt-metathesis in C_6H_6 led to immediate C–H activation of benzene to give ($^{DIPeP}BDI^*$)MgPh and ($^{DIPeP}BDI$)CaH, the latter crystallizing as a THF-solvated dimer $[(^{DIPeP}BDI)CaH{\cdot}THF]_2$. Calculations suggest reduction and insertion of benzene in the Mg–Ca bond. The activation enthalpy for the subsequent decomposition of $C_6H_6^{2-}$ into Ph^- and H^- is only 14.4 kcal mol^{-1}. Repeating this reaction in the presence of naphthalene or anthracene led to heterobimetallic complexes in which naphthalene^{2-} or anthracene^{2-} anions are sandwiched between ($^{DIPeP}BDI^*$)Mg$^+$ and ($^{DIPeP}BDI$)Ca$^+$ cations. These complexes slowly decompose to their homometallic counterparts and further decomposition products. Complexes in which naphthalene^{2-} or anthracene^{2-} anions are sandwiched between two ($^{DIPeP}BDI$)Ca$^+$ cations were isolated. The low-valent complex ($^{DIPeP}BDI^*$)Mg–Ca($^{DIPeP}BDI$) could not be isolated due to its high reactivity. There is, however, strong evidence that this heterobimetallic compound is a fleeting intermediate.

Introduction

Low-valent Mg^I complexes like **I** (Scheme 1) are kinetically stabilized towards disproportionation (2 Mg^I → Mg^{II} + Mg^0) by a bulky β-diketiminate ligand (BDI). Ever since this first milestone discovery by Jones in 2007,[1] there has been quite some interest to isolate other alkaline-earth metals (Ae) in unusually low oxidation states.[2–5] Examples of this activity are the Ca^I inverse sandwich complex **II** by Westerhausen and coworkers,[6] or the Be^0 (**III**) and Be^I (**IV**) complexes by the Braunschweig and Gilliard groups, respectively.[7,8] Since the oxidation state of the Ca metals in **II** depends on the electronic state and charge on the triphenyl-benzene anion, there is some controversy about the Ca valency in this complex.[9] On a similar note, also the oxidation states in CAAC complexes **III** and **IV** are the subject of discussion.[10–13] Early attempts to isolate (BDI)Ca–Ca(BDI) complexes in which the +I oxidation state on the metal is unambiguous hitherto failed.[14] We and others therefore designed BDI ligands with either very large substituents or electron-donating arms aiming to stabilize the larger Ca^I centres.[15–18] Our approach to introduce a ligand without acidic protons in direct vicinity of the metal led to the superbulky $^{DIPeP}BDI$ ligand ($^{DIPeP}BDI$ = HC[C(Me)N-DIPeP]$_2$; DIPeP = 2,6-CH(Et)$_2$-phenyl).[19] The highly dynamic (Et)$_2$CH-substituents in this ligand are relatively inert to deprotonation by strong bases and increase the solubility of its metal complexes in inert (unreactive) solvents like alkanes. Alkane solubility is an important requirement for the isolation of highly reducing low-valent Ae metal complexes.

Previous attempts to prepare (BDI)Ca–Ca(BDI) or (BDI)Sr–Sr(BDI) complexes in aromatic solvents led to solvent reduction and formation of complexes with bridging $C_6H_6^{2-}$ dianions (**V**).[15,20] The extreme reducing power of (BDI)Ca–Ca(BDI) complexes was further demonstrated by isolation of the N_2-activated complex **VI** when alkanes were used as the solvent and N_2 as an "inert" gas.[15] Similar N_2 reduction to N_2^{2-} was found in an attempt to isolate a mixed-metal Ca^I/K^I complex.[17] Attempting the syntheses of (BDI)Ca–Ca(BDI) complexes under an Ar atmosphere led to intractable mixtures of decomposition products.[15,16] Although even larger BDI ligands like $^{DIPeP}BDI^*$ (HC[C(*t*Bu)N-DIPeP]$_2$) so far did not unlock the challenging isolation of (BDI)Ca–Ca(BDI) complexes, this superbulky ligand was successful in the isolation of the first Mg^0 complexes (**VII** and **VIII**).[21]

Inorganic and Organometallic Chemistry, Friedrich-Alexander-Universität Erlangen-Nürnberg, Egerlandstraße 1, Erlangen 91058, Germany. E-mail: sjoerd.harder@fau.de

† Dedicated to Professor Doug Stephan on the occasion of his 70th birthday.

‡ Electronic supplementary information (ESI) available: Crystallographic details including ORTEP plots, ^{1}H and ^{13}C NMR spectra, details for the DFT calculations including XYZ-files. CCDC 2240705–2240709. For ESI and crystallographic data in CIF or other electronic format see DOI: https://doi.org/10.1039/d3sc00909b

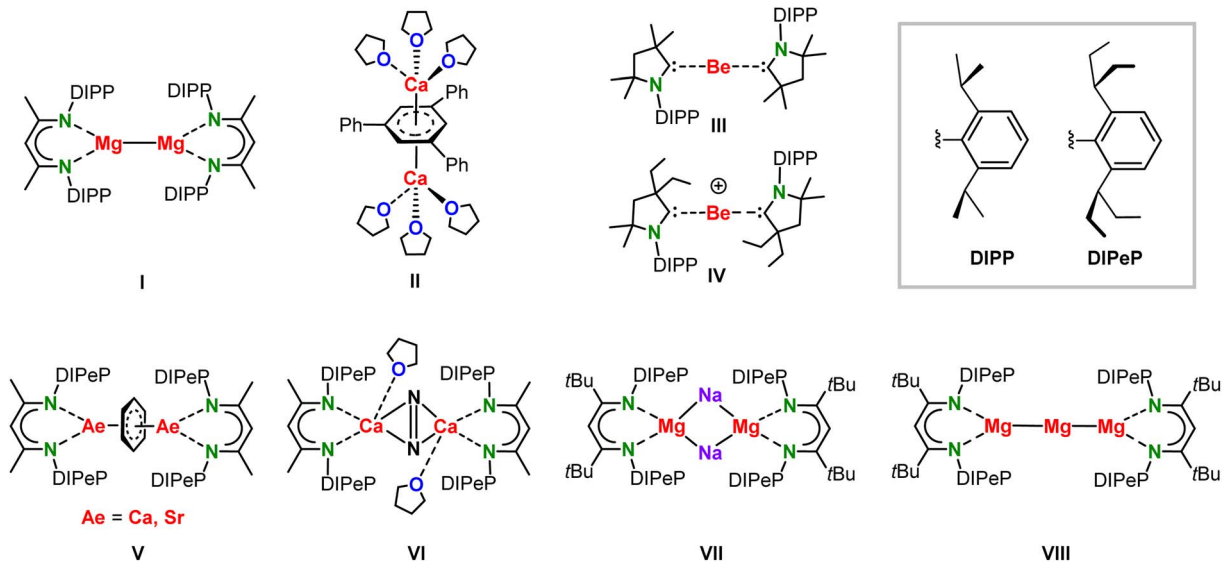

Scheme 1 Complexes I–VIII.

The fair stability of the Mg–Mg bond and the very high reactivity of proposed but so far never isolated (BDI)Ca–Ca(BDI) complexes, begged the question whether mixed-metal (BDI)Mg–Ca(BDI) complexes may be stable. The slight difference in the Mg and Ca electronegativities (Mg 1.31, Ca 1.00)[22] would formally make this a Mg^0/Ca^{II} combination but large electron densities should be expected on both metals. Although there is rare theoretical work on fictitious species with mixed-metal Mg–Be or Mg–Ca bonds,[23,24] the chemistry of mixed low-valent Mg/Ca complexes is hitherto no-man's-land. We here report our theoretical and experimental journey regarding low-valent complexes featuring a Mg–Ca bond.

Results and discussion

DFT-Calculations show that the isolation of low-valent mixed-metal Mg/Ca complexes may be feasible (Scheme 2). Starting from the radicals (^{DIPP}BDI)Mg$^{\bullet}$ and (^{DIPP}BDI)Ca$^{\bullet}$, the energies for formation of the homo- and hetero-metallic low-valent complexes were calculated (^{DIPP}BDI = HC[C(Me)N-DIPP]$_2$; DIPP = 2,6-CH(Me)$_2$-phenyl). Using the B3PW91/def2TZVP//def2SVP level of theory, structures were optimized with and without consideration of dispersion using Grimme's third dispersion correction with Becke–Johnson damping (GD3BJ) (see ESI‡ for details).

Note that correction for attractive dispersive forces between the ^{DIPP}BDI ligands has a considerable effect on the metal–metal bond distances, resulting in shorter and stronger Ae–Ae bonds. Use of dispersion calculates a Mg–Mg bond length (2.882 Å) that is close to the experimentally found value (2.846(1) Å).[1] The calculated energies of formation (ΔH = −55.8 kcal mol^{-1}, ΔG(298 K) = −35.9 kcal mol^{-1}) are in agreement with previously reported Mg–Mg bond energies varying between 36–45 kcal mol^{-1}.[25,26] Unique for the Mg–Mg bond is the occurrence of a Non-Nuclear-Attractor (NNA) in the bond center.[27,28] Experimental electron count in this local maximum of electron density shows a basin with 0.81*e*. This fits very well with the calculated value of 0.80*e* when dispersion correction was used; See Fig. S58‡ for an Atoms-In-Molecules analysis (AIM). Without correction for dispersion a significantly smaller NNA basin of 0.62*e* was calculated (Fig. S59‡). This is in agreement with the observation that the NNA is sensitive to the Mg–Mg distance.[27] Our calculations also show why it is problematic to isolate (BDI)Ca–Ca(BDI) complexes. Even with inclusion of dispersion the Ca–Ca bond is long (3.549 Å) and the bond formation energies are small (ΔH =

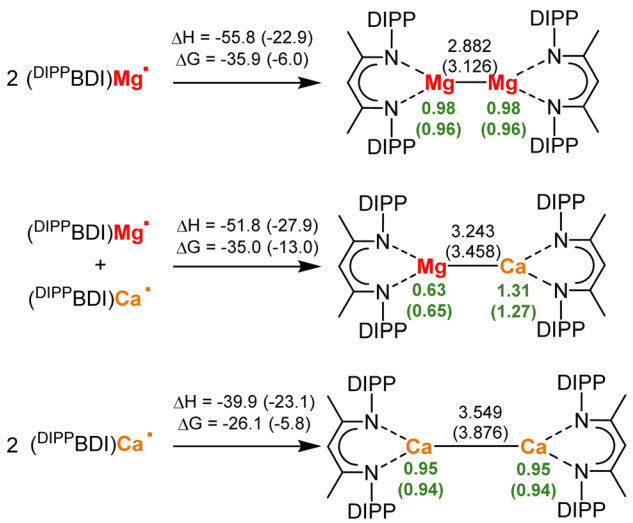

Scheme 2 Formation of homo- and hetero-metallic (^{DIPP}BDI)Ae–Ae(^{DIPP}BDI) complexes (Ae = Mg or Ca). Enthalpies and Gibbs free energies at 298 K in kcal mol^{-1}, Ae–Ae distances in Å and NPA charges in green; B3PW91/def2TZVP//def2SVP with dispersion correction (GD3BJ). Values in brackets relate to calculations without dispersion corrections.

−39.9 kcal mol^{-1}, ΔG(298 K) = −26.1 kcal mol^{-1}). AIM analysis of (^{DIPP}BDI)Ca–Ca(^{DIPP}BDI) shows a regular Ca–Ca bond path with a bond-critical-point in the center. A NNA could not be located. Interestingly, the much longer Ca–Ca bond (3.876 Å) optimized without correction for dispersion, shows a NNA but only with a rather small basin of 0.33*e* (Fig. S61‡). As expected, the Mg–Ca distance in (^{DIPP}BDI)Mg–Ca(^{DIPP}BDI) fits nicely between the values for the Mg–Mg and Ca–Ca bonds. However, surprising is the fact that the Mg–Ca bond in this heterometallic complex is calculated to be nearly as stable as the Mg–Mg bond. Using dispersion, the following Mg–Ca bond formation energies have been calculated: ΔH = −51.8 kcal mol^{-1}, ΔG(298 K) = −35.0 kcal mol^{-1}, values that are close to those for a Mg–Mg bond. AIM analysis on this mixed metal compound does not show the existence of a NNA on the Mg–Ca axis (Fig. S62 and S63‡). Note that metal exchange between the homometallic Mg^{I} and Ca^{I} dimers to give heterometallic (^{DIPP}BDI)Mg–Ca(^{DIPP}BDI) is exothermic and exergonic (ΔH = −7.9 kcal mol^{-1}, ΔG(298 K) = −8.0 kcal mol^{-1}). This distinct thermodynamic preference for the mixed Mg–Ca complex may originate from polarization of the Mg–Ca bond electron density, resulting in a more favorable electrostatic interaction. Indeed, the NPA charges on Mg (+0.63) and Ca (+1.31) clearly show strong polarization towards a Mg^{0}/Ca^{II} complex, however, there is still a considerable electron density on Ca (NPA charges on Ca in regular Ca^{II} complexes are circa +1.75).

The recently reported [(^{DIPeP}BDI*)Mg^{-}Na^{+}]$_2$ complex (**VII**) could be the key to the synthesis of such heterobimetallic complexes. Being a sodium salt of a magnesyl anion, the question arose whether a simple salt-metathesis reaction with the previously reported[11] dimer [(^{DIPeP}BDI)CaI]$_2$ (**IX**) may give access to a mixed-metal low-valent species (^{DIPeP}BDI*)Mg–Ca(^{DIPeP}BDI) featuring a Mg–Ca bond. Although two different metals (Mg and Ca) and two different ligands (^{DIPeP}BDI and ^{DIPeP}BDI*) could result in complications due to metal–ligand scrambling, we have chosen to use the somewhat smaller ^{DIPeP}BDI ligand at Ca for steric reasons. The structure of a recently reported Mg^{I} complex with two superbulky ligands, (^{DIPeP}BDI*)Mg–Mg(^{DIPeP}BDI*), is overcrowded causing one of the BDI ligands to be only monodentate.[22]

Salt-metathesis between **VII** and **X** in methylcyclohexane did not lead to NaI precipitation and the expected product (^{DIPeP}BDI*)Mg–Ca(^{DIPeP}BDI) (**1**); see Scheme 3. ^{1}H NMR in this solvent showed that there is essential no interaction between both dimers. We believe that this is due to complete steric saturation of the metal centers. This is the reason why the vast

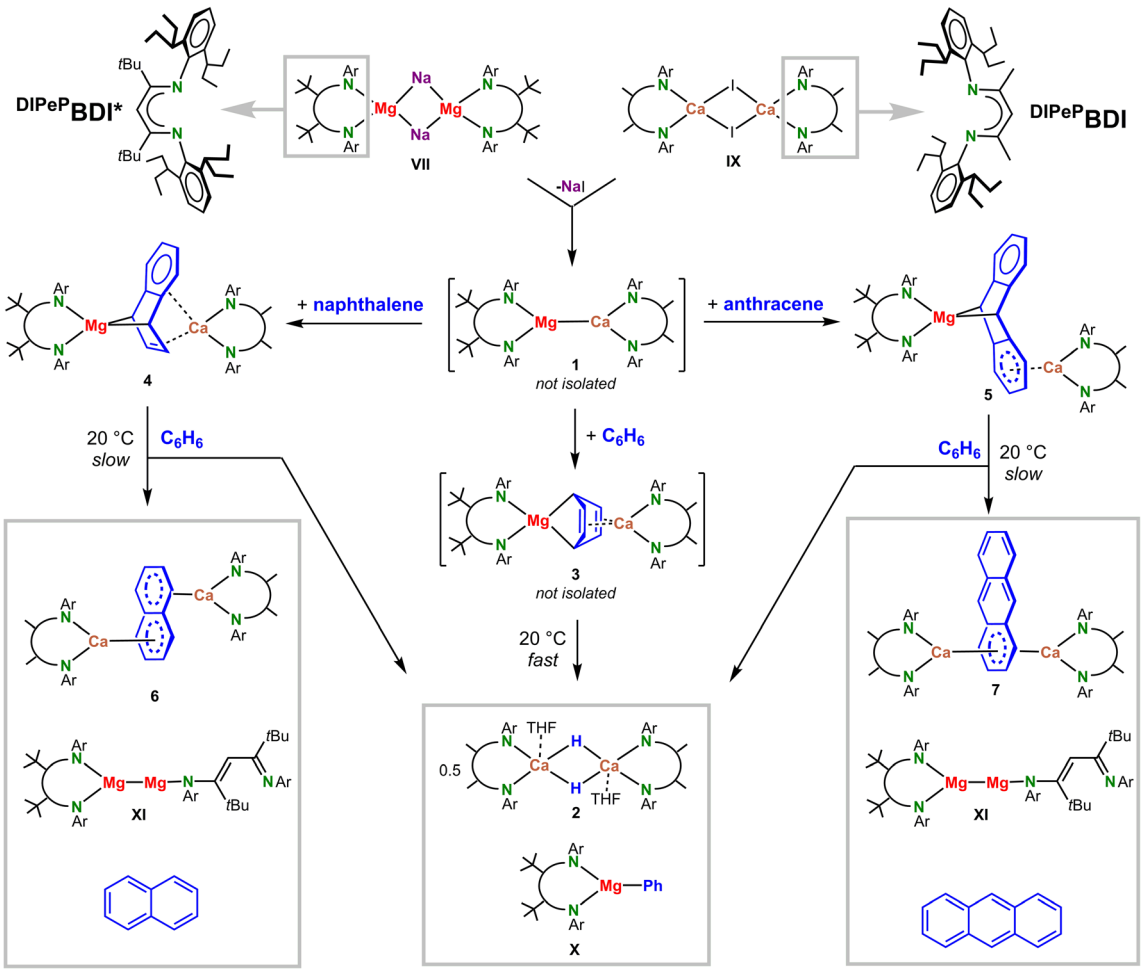

Scheme 3 *In situ* formation, decomposition and reactivity of a low-valent heterobimetallic (BDI)Mg–Ca(BDI) intermediate.

majority of salt-metathesis reactions in s-block metal chemistry are performed in ethereal solvents (preferably THF) that break down aggregates, allowing an encounter between the metal centers of both adducts.

Unfortunately, the sodium magnesyl complex **VII** is not stable in ethers.[21] Recently, successful solid-state salt-metathesis reactions in a ball-mill have been reported.[29] A solvent-free reaction between **VII** and **X** in the ball-mill gave conversion, however, a mixture of various undefined products was formed. Salt-metathesis in the slightly more polar solvent toluene also gave various intractable products but reaction in benzene was selective. A benzene solution of [(^{DIPeP}BDI*)$Mg^{-}Na^{+}$]$_2$ (**VII**) and [(^{DIPeP}BDI)CaI]$_2$ (**IX**) slowly changed color from dark-brown to yellow and over a two-day period a precipitate of NaI was formed. ^{1}H NMR of the crude product showed selective formation of two main species: (^{DIPeP}BDI*)MgPh (**X**), which we previously fully characterized,[21] and (^{DIPeP}BDI)CaH, which after addition of small amounts of THF crystallized as the dimer [(^{DIPeP}BDI)CaH·(THF)]$_2$ (**2**) in 37% yield. The crystal structure of this dimer (Fig. S46‡) resembles the previously reported tetrahydropyran complex.[15] The benzene solvent is the source of the Ph anion in **X** and the hydride in **2**: reaction in C_6D_6 led to the same products with $C_6D_5^-$ and D^- anions (Fig. S30–S32‡).

Cleavage of the C–H bond in benzene has also been observed for previously reported (BDI)Mg(μ^2,μ^4-C_6H_6)Mg(BDI) complexes (formed by reduction of (BDI)MgI in the presence of TMEDA or by ball-milling),[19,30] however, this process needs high temperatures and very long reaction times. Although homometallic (BDI)Mg–Mg(BDI) complexes do not react with benzene, activation of the Mg–Mg bond by UV-light[31] or by a Pd^0 catalyst[32] also led to benzene C–H bond cleavage. In contrast, recently

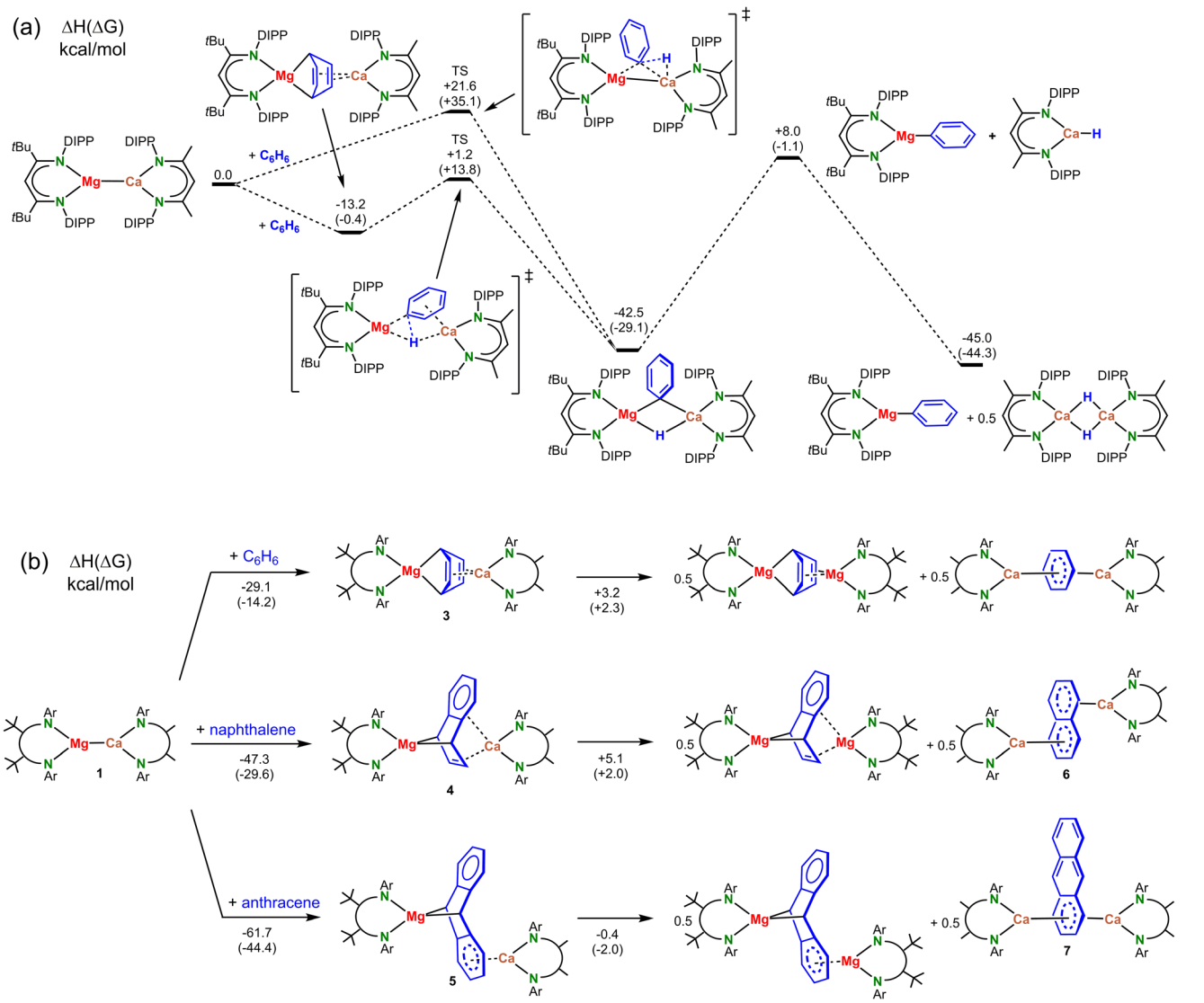

Scheme 4 (a) Calculated mechanism for benzene C–H activation at a low-valent heterobimetallic (BDI)Mg–Ca(BDI) intermediate; B3PW91/def2TZVP//def2SVP with dispersion correction (GD3BJ). (b) Enthalpies and free energies (298 K) for the reaction of (^{DIPeP}BDI*)Mg–Ca(^{DIPeP}BDI) (**1**) with benzene, naphthalene or anthracene and energies for metal exchange to homometallic complexes. Δ*H* and Δ*G* (between parentheses) are given in kcal mol^{-1}.

isolated Ca and Sr complexes with a μ^6-bridging $C_6H_6^{2-}$ ion (**V**) reacted with benzene by dehydrogenative C–C coupling to give a biphenyl^{2-} ion.[20] For the Mg/Ca combination, we found no indication of biphenyl formation.

These observations demonstrate the importance of solvent effects in salt-metathesis reactions. Although there is currently no proof that benzene lowers the aggregation number of **VII** and **X** (DOSY measurements were inconclusive), it is assumed that aromatic (co)solvents influence dimer-monomer equilibria by coordination to the s-block metal. Strong interactions between Ae metal cations and π-systems have been reported[33–37] and are also supported by DFT calculations (Fig. S52‡). Minor quantities of monomeric adducts would enable salt-metathesis between **VII** and **X** to give (^{DIPeP}BDI*)Mg–Ca(^{DIPeP}BDI) (**1**).

Although we found no direct proof for Mg–Ca bond formation, the fleeting existence of such an intermediate seems reasonable. The alternative, formation of (BDI)Mg$^{\bullet}$ and (BDI)Ca$^{\bullet}$ radicals, can be excluded. The (BDI)Mg$^{\bullet}$ radical may react with benzene[26] but would also couple to unreactive dimers, whereas a (BDI)Ca$^{\bullet}$ radical reacts with benzene to a stable complex with a bridging $C_6H_6^{2-}$ dianion (**V**).[15] Both products could not be observed. Instead, selective cleavage of the benzene C–H bond was achieved.

We propose a mechanism in which the expected heterobimetallic intermediate [(^{DIPeP}BDI*)Mg–Ca(^{DIPeP}BDI)] (**1**) reduces benzene to give a complex with a Mg(μ^2,μ^4-C_6H_6)Ca bridge (**3**). DFT-calculations on a model system with DIPP-substituents show that reduction of benzene to give **3** is exothermic by −13.2 kcal mol^{-1} (Scheme 4a).

The smaller Mg^{2+} cation bridges two C atoms in *para*-positions and forms strongly polar Mg–C bonds to the non-aromatic ring. The larger more electropositive Ca^{2+} ion is electrostatically bound to localized C=C bonds. Exchanging Mg and Ca in **3** is unfavorable: a structure with two Ca–C bonds and Mg^{2+}-alkene interactions is 16.1 kcal mol^{-1} higher in energy (Fig. S51‡). Starting from the most stable μ^2,μ^4-bridged benzene complex, the transition state for subsequent C–H bond cleavage is only +14.4 kcal higher in energy. Alternatively, benzene could directly react with the polar Mg–Ca bond but this transition state is more than 20 kcal mol^{-1} higher in energy. Starting from the heterometallic Mg–Ca complex, cleavage of the benzene C–H bond to monomeric (BDI)MgPh and the dimeric Ca hydride complex, is quite exothermic (−45.0 kcal mol^{-1}). Combined with a low activation energy for this process, a complex with a Mg–Ca bond is clearly not stable in benzene.

Since we were unable to isolate the proposed intermediates [(^{DIPeP}BDI*)Mg–Ca(^{DIPeP}BDI)] (**1**) or [(^{DIPeP}BDI*)Mg(μ^2,μ^4-C_6H_6)Ca(^{DIPeP}BDI)] (**3**), we attempted to prepare the more stable naphthalene and anthracene complexes. DFT calculations (Scheme 4b) predict that the reduction of arenes by a Mg–Ca model complex is increasingly more exergonic along the row benzene (ΔG = −14.2 kcal mol^{-1}) < naphthalene (ΔG = −29.6 kcal mol^{-1}) < anthracene (ΔG = −44.4 kcal mol^{-1}).

Repeating the salt-metathesis reaction between [(^{DIPeP}BDI*)Mg$^-$Na$^+$]$_2$ (**VII**) and [(^{DIPeP}BDI)CaI]$_2$ (**IX**) in either methylcyclohexane or benzene in the presence of two equivalents of naphthalene led to a deep purple solution. The crude product is an essentially pure complex (Fig. S33 and S34‡), which after solvent removal and crystallization from pentane at −20 °C, could be isolated in form of orange crystals. The low yield of 29% is due to its very high solubility in pentane. Crystal structure determination shows a heterobimetallic inverse Mg/Ca sandwich with a bridging, non-planar, naphthalene dianion (^{DIPeP}BDI*)Mg(μ^2,μ^4-naphthalene)Ca(^{DIPeP}BDI) (**4**); Fig. 1a and Table 1. The smaller Mg^{2+} cation bridges two C atoms in *para*-positions and forms covalent but strongly polar Mg–C bonds to the non-aromatic ring. The larger more electropositive Ca^{2+} ion is ionically bound to a localized C=C bond and the ring π-system. The Mg^{2+} ion is encapsulated by ^{DIPeP}BDI* whereas the Ca^{2+} ion resides in the pocket of the ^{DIPeP}BDI ligand. There is no indication of metal or ligand exchange. There is also no sign of metal disorder in the crystal structure, illustrating that the Mg and Ca metals are strongly bound in the BDI-ligand pockets. Calculated NPA charges are in agreement with an inverse sandwich consisting of a naphthalene^{2-} ion and Mg^{2+}/Ca^{2+} ions (Fig. 1a).

In a similar procedure, salt-metathesis between **VII** and **IX** in the presence of anthracene yielded red crystals of (^{DIPeP}BDI*)Mg(μ^2,μ^4-anthracene)Ca(^{DIPeP}BDI) (**5**) in 45% yield. Also in this case, the raw product of the reaction is nearly pure (Fig. S35 and S36‡). In contrast to **4**, Mg and Ca in **5** are bound to different rings (Fig. 1b). The Mg^{2+} ion bridges the 9,10-positions of anthracene in a similar fashion as found in Mg(anthracene)·(THF)$_3$, however, the Mg–C distances in **5** (2.374(4) Å and 2.426(4) Å) are somewhat longer (*cf.* 2.25(1)-2.33(1) Å) due the bulk of the BDI ligands.[38] In both Mg-anthracene complexes, the anthracene^{2-} ion is strongly deformed from planarity illustrating dearomatization of the central ring. Loss of aromatic character is also indicated by the C–C distances and AIM analysis (Fig. S55, S65 and S66‡). The much larger Ca^{2+} ion is coordinating to the π-system of one of the outer aromatic rings. This leads to asymmetry and considerable polarization of negative charge to the Ca-bound ring (see Fig. 1b for NPA charges). Delocalization of negative charge is indicated by significantly shorter (Mg)C–C(Ar) bonds in the Ca-bound ring (1.442(5) and 1.444(5) Å) in comparison to those in the free ring (1.470(6) and 1.474(6) Å). A similar coordination mode was also found by the Jones group for the anthracene dianion sandwiched between (^{Mes}BDI)Mg$^+$ cations (Mes = mesityl).[39] It should, however, be noted that the potential energy surface for Ae^{2+} coordination to naphthalene or anthracene dianions is rather shallow and enthalpy differences between different isomers only vary between 2 and 15 kcal mol^{-1} (Fig. S51‡). This is in agreement with the ^{1}H NMR spectrum of the anthracene complex **5** (Fig. S12‡) which shows one signal for the bridgehead Mg–CH protons (3.43 ppm) and two broad signals for the aromatic ring protons (5.13/5.72 ppm), indicating fast exchange of Ca between the two aromatic rings. Cooling to −70 °C led to slow exchange and decoalescence, resulting in five signals for the anthracene^{2-} ion (Fig. S41‡), showing that also in solution an asymmetric structure is favored.

The naphthalene and anthracene complexes **4** and **5** both decompose slowly in solution at room temperature. A purple

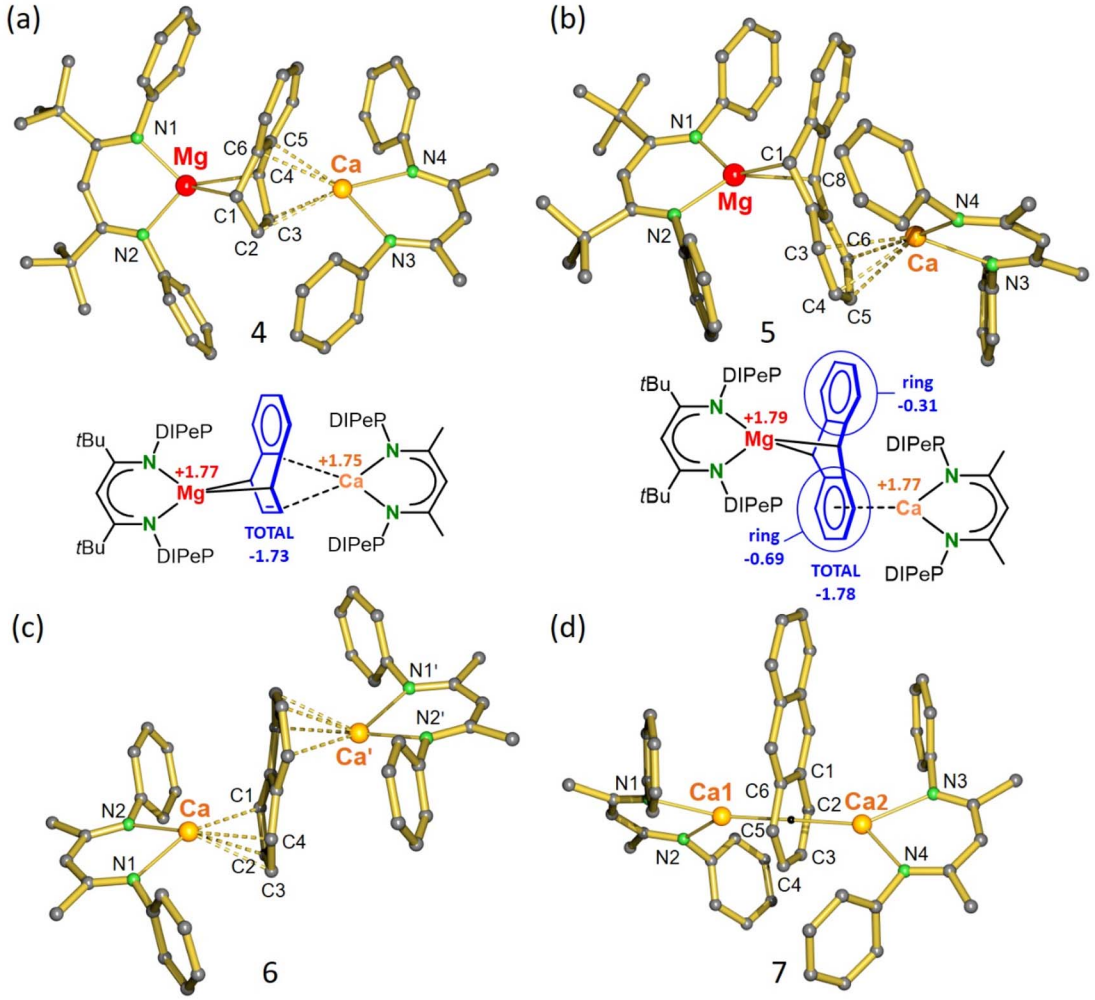

Fig. 1 (a) Crystal structure and NPA charges for (^{DIPeP}BDI*)Mg(μ^2,μ^4-naphthalene)Ca(^{DIPeP}BDI) (**4**). (b) Crystal structure and NPA charges for (^{DIPeP}BDI*)Mg(μ^2,μ^4-anthracene)Ca(^{DIPeP}BDI) (**5**). (c) Crystal structure of (^{DIPeP}BDI)Ca(μ^4,μ^4-naphthalene)Ca(^{DIPeP}BDI) (**6**). (d) Crystal structure of (^{DIPeP}BDI)Ca(μ^6,μ^6-anthracene)Ca(^{DIPeP}BDI) (**7**). All Et_2CH-substituents and H atoms have been omitted for clarity. Selected bond distances are summarized in Table 1.

C_6D_6 solution of the naphthalene complex (**4**) turned blue and was after two weeks fully decomposed. The ^{1}H NMR spectra show formation of several species (Fig. S37 and S38‡). After 13 days, the main decomposition product was characterized as the naphthalene dianion sandwiched between two (^{DIPeP}BDI)Ca$^+$ ions (**6** and Fig. 1c). This complex could also be obtained by an independent synthetic procedure in the form of blue crystals (*vide infra*). Its formation suggests scrambling of the heterobimetallic Mg/Ca complex **4** to give the homometallic Mg/Mg and Ca/Ca analogues. Although the homometallic complex

Table 1 Selected bond distances (Å) for complexes **4**–**7**

Complex **4**	Complex **5**	Complex **6**	Complex **7**	
Mg–N1 2.112(1)	Mg–N1 2.109(3)	Ca–N1 2.330(1)	Ca1–N1 2.345(1)	Ca2–N3 2.348(1)
Mg–N2 2.095(1)	Mg–N2 2.128(3)	Ca–N2 2.365(1)	Ca1–N2 2.338(1)	Ca2–N4 2.338(1)
Mg–C1 2.344(1)	Mg–C1 2.374(4)	Ca–C1 2.642(1)	Ca1–C1 2.776(2)	Ca2–C1 2.706(1)
Mg–C4 2.376(1)	Mg–C8 2.426(4)	Ca–C2 2.654(1)	Ca1–C2 2.715(1)	Ca2–C2 2.708(2)
Ca–N3 2.345(1)	Ca–N3 2.341(3)	Ca–C3 2.673(1)	Ca1–C3 2.704(1)	Ca2–C3 2.726(2)
Ca–N4 2.357(1)	Ca–N4 2.338(3)	Ca–C4 2.674(1)	Ca1–C4 2.696(1)	Ca2–C4 2.717(2)
Ca–C2 2.839(2)	Ca–C3 2.778(4)		Ca1–C5 2.681(2)	Ca2–C5 2.702(1)
Ca–C3 2.732(2)	Ca–C4 2.724(4)		Ca1–C6 2.746(2)	Ca2–C6 2.715(1)
Ca–C5 2.676(1)	Ca–C5 2.744(4)			
Ca–C6 2.825(1)	Ca–C6 2.821(4)			

(^{DIPeP}BDI)Ca(μ^4,μ^4-naphthalene)Ca(^{DIPeP}BDI) (**6**) is the main decomposition product, the fate of Mg is found to be different. Apart from the previously reported Mg^I dimer (^{DIPeP}BDI*)Mg–Mg(^{DIPeP}BDI*) (**XI**),[26] also free naphthalene and typical benzene C–H bond activation products like (^{DIPeP}BDI*)MgPh (**X**) and the Ca hydride complex **2** could be observed by ^{1}H NMR (Fig. S37 and S38‡). This indicates that the naphthalene^{2-} ion in **4** can partially be replaced by the benzene solvent to form **3** and its decomposition products.

A similar decomposition pathway was observed for the anthracene complex **5** (Fig. S39 and S40‡). The main decomposition product was found to be homometallic (^{DIPeP}BDI)Ca(μ^6,μ^6-anthracene)Ca(^{DIPeP}BDI) (**7** and Fig. 1d) which could also be obtained by an independent synthetic procedure in the form of dark-blue crystals (*vide infra*). Other decomposition products are (^{DIPeP}BDI*)Mg–Mg(^{DIPeP}BDI*) (**XI**), free anthracene and typical benzene C–H bond activation products like (^{DIPeP}BDI*)MgPh (**X**) and the Ca hydride complex **2**.

Full decomposition of the heterobimetallic Mg/Ca complexes **4** and **5** in the homobimetallic Ca/Ca complexes **6** and **7** suggests that the mixed-metal combinations is less stable than the homometallic combinations. Calculations show that the energy differences between hetero- and homobimetallic complexes are small and therefore statistical Mg/Ca scrambling could be expected (Scheme 4b). The driving force for metal exchange is therefore dictated by formation of other side products, *e.g.* the cleavage of the benzene C–H bond which according to Scheme 4a is highly exothermic.

Alternatively, the bimetallic Ca complexes of naphthalene (**6**) and anthracene (**7**) could be prepared by reduction of [(^{DIPeP}BDI)CaI]$_2$ (**IX**) with KC_8 in the presence of either naphthalene or anthracene to give the products as intensely blue crystals in reasonable isolated yields (**6**: 46%, **7**: 48%). Their crystal structures differ from those of the heterometallic Mg/Ca complexes **4** and **5** by changes in coordination of the central dianion.

The naphthalene dianion in the centrosymmetric structure of **6** is sandwiched between two Ca^{2+} ions coordinating to different rings (Fig. 1c). Bonding is mainly ionic and the naphthalene dianion is only slightly distorted from its flat aromatic structure. Each six-membered ring is deformed to a butterfly-type structure with an interplanar angle of 14.92(5)°. A similar geometry was reported for the dilithium salt of naphthalene: $(C_8H_8)Li_2\cdot(TMEDA)_2$.[40]

The crystal structure of anthracene complex **7** is close to being C_2-symmetric but has no crystallographic symmetry (Fig. 1d). The Ca atoms bind in η^6-fashion to a common anthracene outer-ring with Ca–C bond distances in a narrow range of 2.681(2)–2.776(2) Å. DFT calculations show that the structure in which the two Ca atoms bind to opposite outer-rings is 13.2 kcal mol^{-1} higher in energy (Fig. S51‡). While preference for **7** is correctly predicted by DFT theory, the crystal structure of the naphthalene complex **6** is not in agreement with the lowest energy structure. DFT calculations predict that also in this case coordination to a common ring is favorable by $\Delta H =$ 14.7 kcal mol^{-1} (Fig. S51‡). We believe that coordination to a common naphthalene or anthracene ring is favored due to very strong polarizability of these extended π-systems. Indeed, in **7** the electron density on the anthracene dianion is mainly on the ring sandwiched by the two Ca^{2+} ions (NPA charge: −1.40) and not on the free outer-ring (NPA charge: −0.20). This results in increased electrostatic attraction between Ca^{2+} and the anthracene dianion. The high electron density on the Ca-bound ring is also evident from the considerably longer C–C bonds (average: 1.441 Å) *vs.* the C–C bonds in the uncoordinated ring (average: 1.399 Å). This originates from partial occupation of anti-bonding π*-orbitals in the Ca-bound ring. In contrast to the Mg/Ca anthracene complex **5**, the relatively shallow potential energy surfaces for Ca/Ca coordination do not allow to freeze out the asymmetric coordination geometry in solution. ^{1}H NMR spectra of **6** and **7** in toluene show down to −70 °C fast exchange between coordination geometries.

Conclusion

Although isolation and structural characterization of a low-valent Ae metal complex with a direct Mg–Ca bond remains a challenge, there are strong indications to assume that such a species has been formed as a fleeting intermediate.

(1) The experimental approach, *i.e.* ion exchange between Mg^-–Na^+ and Ca^+–I^- bonds, implies formation of a Mg–Ca bond and NaI salt which is the driving force of this salt-metathesis reaction. The existence of the free (BDI)Mg$^\bullet$ and (BDI)Ca$^\bullet$ radicals rather than a Mg–Ca bound species can be ruled out, as they would react differently with benzene or other arenes.

(2) DFT-Calculations underscore that the Mg–Ca bond strength is comparable to that of the Mg–Mg bond for which there are numerous verifiable examples.[2–5] These calculations also show that a heterobimetallic (BDI)Mg–Ca(BDI) complex is thermodynamically favored over its homometallic Mg/Mg and Ca/Ca counterparts. Polarization of the Mg–Ca bond, however, makes it highly reactive and kinetically unstable. The herein observed reduction of benzene to $C_6H_6^{2-}$ and subsequent C–H bond cleavage can be achieved at room temperature, giving selectively (BDI)Mg–Ph and (BDI)Ca–H complexes. This reaction has been calculated to be highly exothermic ($\Delta H =$ −45.0 kcal mol^{-1}) and has a kinetic barrier of only +14.4 kcal mol^{-1}.

(3) Although the predicted intermediate, (BDI)Mg–(C_6H_6)–Ca(BDI), could not be isolated, similar but more stable complexes with naphthalene^{2-} and anthracene^{2-} ions were obtained by salt-metathesis in the presence of easily reducible naphthalene or anthracene. The naphthalene and anthracene complexes are exclusively formed as mixed-metal Mg/Ca species (**4** and **5**) which over time decompose to more stable homometallic Ca/Ca species (**6** and **7**) and low-valent (BDI)Mg–Mg(BDI). This is indirect proof for prior formation of a low-valent intermediate with two different metals which may feature a Mg–Ca bond.

Reduction of naphthalene or anthracene by a combination of free (BDI)Mg$^\bullet$ and (BDI)Ca$^\bullet$ radicals would at most lead to statistical Mg/Mg, Ca/Ca and Mg/Ca distributions or directly to the more stable homometallic Ca/Ca species (**6** and **7**) and low-valent (BDI)Mg–Mg(BDI). This is indeed the case. Reduction of

an equimolar mixture of (^{DIPeP}BDI*)MgI and (^{DIPeP}BDI)CaI with KC_8 in the presence of naphthalene led only to small amounts of the heterobimetallic Mg/Ca complex **4**. Instead, major quantities of the homometallic Ca/Ca species **6** and low-valent (^{DIPeP}BDI*)Mg–Mg(^{DIPeP}BDI*) (**XI**) were formed (Fig. S45‡). In contrast, salt-metathesis between [(^{DIPeP}BDI*)Mg$^-$Na$^+$]$_2$ (**VII**) and [(^{DIPeP}BDI)CaI]$_2$ (**IX**) in the presence of naphthalene gave clean formation of the heterobimetallic Mg/Ca complex **4**.

Arguably, **4** may also be formed by a two-step mechanism: (a) reduction of naphthalene by [(^{DIPeP}BDI*)Mg$^-$Na$^+$]$_2$ (**VII**) to give (^{DIPeP}BDI*)Mg(naphthalene)Na and (b) subsequent salt-metathesis with [(^{DIPeP}BDI)CaI]$_2$ (**IX**) yielding the heterobimetallic Mg/Ca complex **4** and NaI. Indeed, [(^{DIPeP}BDI*)Mg$^-$Na$^+$]$_2$ (**VII**) reacts with naphthalene to give a dark-orange solution but so far no products could be isolated. Although this order of reactions may be an alternative pathway for naphthalene or anthracene reduction, it cannot be the pathway for benzene reduction: **VII** is not able to reduce benzene. Instead, Na^+ is slowly reduced to Na^0 under simultaneous formation of a trinuclear (BDI)Mg–Mg–Mg(BDI) complex (**VIII**).[21] The cleavage of the C–H bond in benzene to give complexes **2** and **X** must therefore most likely proceed through the low-valent mixed Mg–Ca species (^{DIPeP}BDI*)Mg–Ca(^{DIPeP}BDI), formed by the salt-metathesis reaction of [(^{DIPeP}BDI*)Mg$^-$Na$^+$]$_2$ (**VII**) and [(^{DIPeP}BDI)CaI]$_2$ (**IX**) (Scheme 3). This is further supported by a conceivable calculated mechanism for benzene C–H bond activation (Scheme 4a).

Although a first example of a (BDI)Mg–Ca(BDI) complex could not be isolated, the existence of a highly reactive intermediate with a Mg–Ca bond is plausible. After first reactivity studies with benzene, naphthalene and anthracene, we are currently extending our explorations in heterobimetallic low-valent Mg–Ca chemistry.

Experimental section

General considerations

All experiments were conducted in dry glassware under an inert nitrogen atmosphere by applying standard Schlenk techniques or gloveboxes (MBraun) using freshly dried and degassed solvents. All solvents were degassed with nitrogen, dried over activated aluminum oxide (Innovative Technology, Pure Solv 400-4-MD, Solvent Purification System), and then stored under inert atmosphere over molecular sieves (3 Å) unless noted otherwise. Deuterated benzene (C_6D_6), toluene-d_8, cyclohexane-d_{12} and methylcyclohexane-d_{14} were purchased from Sigma Aldrich or Deutero GmbH, degassed and dried over molecular sieves (3 Å). The following compounds were synthesized according to literature procedures: [(^{DIPeP}BDI*)MgNa]$_2$,[21] [(^{DIPeP}BDI)CaI]$_2$,[15] [(^{DIPeP}BDI)CaH]$_2$ (ref. 15) and [(^{DIPeP}BDI)CaN(SiMe$_3$)]$_2$·(THF).[41] $PhSiH_3$ (Alfa Aesar, >99%) was obtained commercially as well as, naphthalene (Sigma Aldrich, 99%) and anthracene (Sigma Aldrich, 97%) which were sublimed under reduced pressure and stored under an N_2 atmosphere. NMR spectra were measured on Bruker Avance III HD 400 MHz and Bruker Avance III HD 600 MHz spectrometers. Chemical shifts (δ) are denoted in ppm (parts per million), coupling constants in Hz (Hertz). For describing signal multiplicities common abbreviations are used: s (singlet), d (doublet), t (triplet), q (quartet), p (quintet), sept (septet), m (multiplet) and br (broad). Spectra were referenced to the solvent residual signal. Assignments of resonance signals in the ^{1}H and ^{13}C{^{1}H} NMR spectra were made based on two-dimensional NMR correlation (HSQC, HMBC, COSY) experiments. Elemental analysis was performed with an Hekatech Eurovector EA3000 analyzer. All crystal structures have been measured on a SuperNova (Agilent) diffractometer with dual Cu and Mo microfocus sources and an Atlas S2 detector. Crystallographic data have been deposited with the Cambridge Crystallographic Data Centre as supplementary publication numbers: CCDC 2240705 [(^{DIPeP}BDI)CaH·(THF)]$_2$ (**2**), 2240706 (^{DIPeP}BDI*)Mg(μ^2,μ^4-naphthalene)Ca(^{DIPeP}BDI) (**4**), 2240707 (^{DIPeP}BDI*)Mg(μ^2,μ^4-anthracene)Ca(^{DIPeP}BDI) (**5**), 2240708 (^{DIPeP}BDI)Ca(μ^4,μ^4-naphthalene)Ca(^{DIPeP}BDI) (**6**), 2240709 (^{DIPeP}BDI)Ca(μ^6,μ^6-anthracene)Ca(^{DIPeP}BDI) (**7**).

Synthesis of [(^{DIPeP}BDI)CaH·(THF)]$_2$ (2). Method A: in a J.-Young tube [(^{DIPeP}BDI*)MgNa]$_2$ (28.7 mg, 0.0220 mmol) and [(^{DIPeP}BDI)CaI]$_2$ (31.3 mg, 0.0220 mmol) were dissolved in C_6H_6 (1 mL). Stirring the mixture at room temperature for two days led to a colorless precipitate and a yellow solution. The solvent was removed, and the residue was stripped with pentane (1 × 1 mL) and dissolved in pentane (0.7 mL). After filtration of the slightly cloudy solution, THF (1.87 μL, 0.0231 mmol) was added. Subsequently the solution was stored at −30 °C for crystallization. After five hours colorless crystals of [(^{DIPeP}BDI)CaH·(THF)]$_2$ were grown. The supernatant was decanted, the crystals washed with cold pentane (−20 °C, 1 × 0.3 mL) and dried *in vacuo*. Yield: 10.6 mg (0.00824 mmol, 37%). Method B: THF-free [(^{DIPeP}BDI)CaH]$_2$ (328 mg, 0.287 mmol) was dissolved in hexane (600 μL). THF (50 μL, 0.610 mmol), diluted with hexane (150 μL), was added without stirring. Leaving it standing overnight at ambient temperature gave colorless crystals of [(^{DIPeP}BDI)CaH·(THF)]$_2$ suitable for X-ray diffraction analysis. The supernatant was decanted, and the crystals dried under high vacuum. A second crop of crystals was obtained by cooling the mother liquor at −20 °C overnight. Overall yield: 310 mg (0.241 mmol, 84%). Method C: [(^{DIPeP}BDI)CaN(SiMe$_3$)$_2$·(THF)] (850 mg, 1.06 mmol) was dissolved in hexane (3 mL) and the solution was cooled to −80 °C. At this temperature $PhSiH_3$ (391 μL, 3.18 mmol) dissolved in hexane (500 μL) was added dropwise *via* a syringe. The solution was allowed to warm to room temperature overnight yielding an orange suspension. The colorless microcrystalline solid was isolated by centrifugation, quickly washed with cold pentane (−20 °C, 2 × 0.5 mL) and dried under high vacuum to give [(^{DIPeP}BDI)CaH·(THF)]$_2$ (136 mg). Cooling the mother liquor overnight at −20 °C gave another crop of colorless crystals of [(^{DIPeP}BDI)CaH·(THF)]$_2$ which were isolated by decantation, quickly washed with cold pentane (−20 °C, 2 × 0.5 mL) and dried *in vacuo*. Combined yield: 422 mg (0.660 mmol, 62%). ^{1}H NMR (400 MHz, C_6D_6, 298 K): δ = 7.03–7.12 (m, 6H, C*H*-arom), 4.77 (s, 1H, C*H*-backbone), 4.11 (s, 1H, Ca–*H*), 3.56–3.60 (m, 4H, OCH_2CH$_2$), 2.66 (quint, ^{3}J = 6.6 Hz, 4H, C*H*), 1.67 (s, 6H, CH_3-backbone), 1.57–1.69 (m, 8H, CH_2), 1.45–1.56 (m, 8H, CH_2), 1.40–1.44 (m, 4H, OCH$_2$CH_2),

0.86 (t, ^{3}J = 7.4 Hz, 12H, CH_3), 0.82 (t, ^{3}J = 7.4 Hz, 12H, CH_3) ppm. ^{13}C NMR (101 MHz, C_6D_6, 298 K): δ = 165.5 (*C*N-backbone), 147.4 (*C*-arom), 140.0 (*C*-arom), 125.0 (*C*-arom), 124.0 (*C*-arom), 93.7 (*C*H-backbone), 67.9 (O*C*H_2CH$_2$), 42.2 (*C*H), 29.5 (*C*H_2), 26.7 (*C*H_2), 25.8 (OCH$_2$*C*H_2), 24.7 (*C*H_3-backbone), 13.6 (*C*H_3), 12.1 (*C*H_3) ppm. Elemental analysis for $C_{82}H_{132}Ca_2N_4O_2$ (M = 1286.14 g mol^{-1}): C 76.58, H 10.35, N 4.36%. Found: C 76.62, H 10.36, N 4.36%.

Synthesis of (^{DIPeP}BDI*)Mg(μ^2,μ^4-naphthalene)Ca(^{DIPeP}BDI) (4). In a J.-Young tube [(^{DIPeP}BDI*)MgNa]$_2$ (80.0 mg, 0.0610 mmol), [(^{DIPeP}BDI)CaI]$_2$ (84.0 mg, 0.0600 mmol) and naphthalene (16.0 mg, 0.125 mmol) were dissolved in C_6D_6 or methylcyclohexane (600 μL). The mixture turned immediately purple and was stirred at room temperature for one hour. The solvent was removed under vacuum and the purple residue was dissolved in pentane (2 mL) and slowly cooled to −20 °C for crystallization. After one day, orange crystals were isolated by decantation, washed with cold pentane (2 × 300 μL) and dried *in vacuo*. Crystalline yield: 48.0 mg (0.0359 mmol, 29%). ^{1}H NMR (C_6D_6, 400 MHz, 298 K): δ = 7.10–7.02 (m, 6H, C*H*-arom), 6.94–6.92 (m, 6H, C*H*-arom), 5.24 (s, 1H, C*H*-backbone), 5.18 (br s, 2H, C*H*-napht), 4.75 (s, 1H, C*H*-backbone), 4.69 (s, 2H, C*H*-napht), 3.61 (br s, 2H, C*H*-napht), 3.12 (sept, $^3J_{HH}$ = 3.8 Hz, 4H, C*H*), 2.65 (br s, 2H, C*H*-napht), 2.50 (p, $^3J_{HH}$ = 5.9 Hz, 4H, C*H*), 1.98–1.91 (m, 8H, CH_2), 1.89–1.81 (m, 4H, CH_2), 1.92–1.84 (m, 4H, CH_2), 1.78–1.72 (m, 4H, CH_2), 1.64 (s, 6H, CH_3-backbone), 1.63–1.56 (m, 12H, CH_2), 1.23 (s, 18H, C(CH_3)$_3$-backbone), 1.19 (t, $^3J_{HH}$ = 7.3 Hz, 12H, CH_3), 1.07 (t, $^3J_{HH}$ = 7.3 Hz, 12H, CH_3), 1.00 (t, $^3J_{HH}$ = 7.3 Hz, 12H, CH_3), 0.79 (t, $^3J_{HH}$ = 7.3 Hz, 12H, CH_3) ppm. ^{13}C NMR (C_6D_6, 101 MHz, 298 K): δ = 175.1 (s, *C*N-backbone), 165.9 (s, *C*N-backbone), 149.3 (s, *C*-arom), 149.1 (s, *C*-arom), 147.0 (s, *C*-napht), 139.6 (s, *C*-arom), 139.0 (s, *C*-arom), 126.1 (s, *C*-arom), 125.4 (s, *C*-arom), 124.0 (s, *C*-arom), 123.0 (s, *C*-arom), 120.4 (s, *C*H-napht), 112.8 (s, *C*H-napht), 107.3 (s, *C*H-napht), 95.9 (s, *C*H-backbone), 94.4 (s, *C*H-backbone), 66.8 (s, *C*H-napht), 44.4 (s, *C*(CH$_3$)$_3$), 42.5 (s, *C*H), 40.4 (s, *C*H), 33.7 (s, C(*C*H$_3$)$_3$), 28.0 (s, *C*H$_2$), 24.7 (s, *C*H$_2$), 24.3 (s, *C*H$_3$-backbone), 23.9 (s, *C*H$_2$), 12.8 (s, *C*H$_3$), 11.5 (s, *C*H$_3$), 11.1 (s, *C*H$_3$), 10.9 (s, *C*H$_3$) ppm. Elemental analysis for $C_{90}H_{134}CaMgN_4$ (M = 1336.47 g mol^{-1}): C 80.88, H 10.11, N 4.19%. Found: C 80.90, H 10.18, N 4.34%.

Synthesis of (^{DIPeP}BDI*)Mg(μ^2,μ^4-anthracene)Ca(^{DIPeP}BDI) (5). In the glovebox [(^{DIPeP}BDI*)MgNa]$_2$ (214 mg, 0.162 mmol) was dissolved in precooled toluene or methylcyclohexane (4 mL, −20 °C). [(^{DIPeP}BDI)CaI]$_2$ (226 mg, 0.162 mmol) and anthracene (57.8 mg, 0.324 mmol) were also dissolved in precooled toluene or methylcyclohexane (4 mL, −20 °C). Both solutions (brown and yellow) were mixed and immediately a colour change to red occurred. The solvent was removed under vacuum, the remaining red solid was dissolved in pentane (2 mL), filtered and crystallized at −20 °C. After 7 days red crystals of (^{DIPeP}BDI*)Mg(μ^2,μ^4-anthracene)Ca(^{DIPeP}BDI) suitable for X-ray diffraction were isolated by decantation, washed with cold pentane (200 μL) and dried *in vacuo*. Crystalline yield: 75.0 mg (0.0541 mmol, 45%). ^{1}H NMR (C_6D_6, 600 MHz, 298 K): δ = 7.10–7.06 (m, 7H, C*H*-arom), 7.03–7.01 (m, 5H, C*H*-arom), 5.72 (br s, 4H, C*H*-anth), 5.24 (s, 1H, C*H*-backbone), 5.13 (br. s, 4H, C*H*-anth), 4.73 (s, 1H, C*H*-backbone), 3.43 (br s, 2H, C*H*-anth), 3.05–3.03 (m, 4H, C*H*), 2.48–2.44 (m, 4H, C*H*), 1.93–1.90 (m, 4H, CH_2), 1.76–1.71 (m, 4H, CH_2), 1.66 (s, 6H, CH_3-backbone), 1.62–1.51 (m, 24H, CH_2), 1.22 (t, $^3J_{HH}$ = 7.3 Hz, 12H, CH_3), 1.16 (s, 18H, C(CH_3)$_3$-backbone), 0.98 (t, $^3J_{HH}$ = 7.3 Hz, 12H, CH_3), 0.93 (t, $^3J_{HH}$ = 7.3 Hz, 12H, CH_3), 0.72 (t, $^3J_{HH}$ = 7.3 Hz, 12H, CH_3) ppm. ^{13}C NMR (C_6D_6, 151 MHz, 298 K): δ = 175.7 (s, *C*N-backbone), 165.5 (s, *C*N-backbone), 148.9 (s, *C*-arom), 146.3 (s, *C*-arom), 143.2 (s, *C*-anth), 140.1 (s, *C*-arom), 138.8 (s, *C*-arom), 126.0 (s, *C*-arom), 125.4 (s, *C*-arom), 124.0 (s, *C*-arom), 123.4 (s, *C*-arom), 118.9 (s, *C*H-anth), 112.6 (s, *C*H-anth), 97.2 (s, *C*H-backbone), 94.2 (s, *C*H-backbone), 44.5 (s, *C*(CH$_3$)$_3$), 42.0 (s, *C*H), 40.8 (s, *C*H), 33.6 (s, C(*C*H$_3$)$_3$), 27.4 (s, *C*H$_2$), 26.4 (s, *C*H$_2$), 25.0 (s, *C*H$_2$), 24.0 (s, *C*H$_3$-backbone), 23.5 (s, *C*H$_2$), 13.0 (s, *C*H$_3$), 12.9 (s, *C*H$_3$), 10.8 (s, *C*H$_3$), 10.6 (s, *C*H$_3$) ppm. One C-signal of the anthracene moiety is not visible. Elemental analysis for $C_{94}H_{136}CaMgN_4$ (M = 1386.53 g mol^{-1}): C 81.43, H 9.89, N 4.04%. Found: C 80.84, H 10.24, N 3.78%.

Synthesis of (^{DIPeP}BDI)Ca(μ^4,μ^4-naphthalene)Ca(^{DIPeP}BDI) (6). [(^{DIPeP}BDI)CaI]$_2$ (200 mg, 0.144 mmol), KC_8 (232 mg, 1.72 mmol) and naphthalene (18.5 mg, 0.144 mmol) were suspended in methylcyclohexane (6 mL) and stirred at room temperature overnight. The mixture was filtered, and the deep blue solution was evaporated to dryness. The crude product was stripped with pentane (1 × 1.5 mL), dissolved in pentane (500 μL) and filtered. Leaving it standing overnight at −20 °C gave dark-blue crystals of (^{DIPeP}BDI)Ca(μ^4,μ^4-naphthalene)Ca(^{DIPeP}BDI) suitable for X-ray diffraction analysis. After decantation of the mother liquor, the crystals were washed with cold pentane (−20 °C, 1 × 300 μL) and dried *in vacuo*. Yield: 84 mg (0.0662 mmol, 46%). ^{1}H NMR (C_6D_6, 600 MHz, 298 K): δ = 6.97–6.94 (m, 12H, C*H*-arom), 5.08 (s, 2H, C*H*-backbone), 3.26 (m, 4H, C*H*-napht), 2.96–2.92 (m, 8H, C*H*), 1.93 (t, $^3J_{HH}$ = 4.0 Hz, 4H, C*H*-napht), 1.91 (s, 12H, CH_3-backbone), 1.79 (dq, $^3J_{HH}$ = 14.1, 7.0 Hz, 16H, CH_2), 1.72–1.69 (m, 8H, CH_2), 1.67–1.63 (m, 8H, CH_2), 1.15 (t, $^3J_{HH}$ = 7.3 Hz, 24H, CH_3), 0.88 (t, $^3J_{HH}$ = 7.4 Hz, 24H, CH_3) ppm. ^{13}C NMR (C_6D_6, 151 MHz, 298 K): δ = 165.9 (s, *C*N-backbone), 157.7 (s, *C*-napht), 147.7 (s, *C*-arom), 139.2 (s, *C*-arom), 125.6 (s, *C*-arom), 123.4 (s, *C*-arom), 119.0 (s, C-napht), 94.4 (*C*H-backbone), 89.4 (s, *C*-napht), 42.2 (s, *C*H), 28.1 (s, *C*H$_2$), 25.3 (s, *C*H$_2$), 24.5 (s, *C*H$_3$-backbone), 12.6 (s, *C*H$_3$), 11.4 (s, *C*H$_3$) ppm. Elemental analysis for $C_{84}H_{122}Ca_2N_4$ (M = 1268.08 g mol^{-1}): C 79.56, H 9.70, N 4.42. Found: C 79.33, H 9.89, N 4.21.

Synthesis of (^{DIPeP}BDI)Ca(μ^6,μ^6-anthracene)Ca(^{DIPeP}BDI) (7). [(^{DIPeP}BDI)CaI]$_2$ (400 mg, 0.287 mmol), KC_8 (465 mg, 3.44 mmol) and anthracene (51.1 mg, 0.287 mmol) were suspended in methylcyclohexane (8 mL) and stirred at room temperature overnight. The mixture was filtered, and the blue solution was evaporated to dryness. The crude product was stripped with pentane (1 × 1.5 mL), dissolved in pentane (500 μL) and filtered. Leaving it standing overnight at −20 °C gave dark-blue crystals of (^{DIPeP}BDI)Ca(μ^6,μ^6-anthracene)Ca(^{DIPeP}BDI) suitable for X-ray diffraction analysis. After decantation of the mother liquor, the crystals were washed with cold pentane (−20 °C, 1 × 300 μL) and dried *in vacuo*. Yield: 183 mg (0.139 mmol, 48%). ^{1}H NMR (C_6D_6, 600 MHz, 298 K): δ = 6.97–6.95 (m, 12H, C*H*-arom), 5.08 (s, 2H, C*H*-backbone), 4.37 (m, 4H, C*H*-anth), 3.27 (t, $^3J_{HH}$ = 4.3 Hz, 4H, C*H*-anth), 2.86 (p, $^3J_{HH}$ = 6.2 Hz, 8H, C*H*), 2.10 (s, 2H, C*H*-anth), 1.91 (s, 12H, CH_3-backbone), 1.84–1.80 (m, 16H,

CH_2), 1.65 (q, $^3J_{HH}$ = 7.3 Hz, 16H, CH_2), 1.09 (t, $^3J_{HH}$ = 7.3 Hz, 24H, CH_3), 0.87 (t, $^3J_{HH}$ = 7.3 Hz, 24H, CH_3) ppm. ^{13}C NMR (C_6D_6, 151 MHz, 298 K): δ = 166.1 (s, *C*N-backbone), 147.1 (s, *C*-arom), 145.1 (s, *C*-anth), 139.4 (s, *C*-arom), 125.7 (s, *C*-arom), 123.5 (s, *C*-arom), 119.1 (s, *C*-anth), 103.0 (s, *C*-anth), 94.7 (*C*H-backbone), 91.4 (s, *C*-anth), 42.4 (s, *C*H), 28.0 (s, CH_2), 24.9 (s, CH_2), 24.4 (s, CH_3-backbone), 13.0 (s, CH_3), 11.1 (s, CH_3) ppm. Elemental analysis for $C_{88}H_{124}Ca_2N_4$ (M = 1318.14 g mol^{-1}): C 80.19, H 9.48, N 4.25; Found: C 80.37, H 9.43, N 4.29.

Data availability

Crystallographic data has been deposited with the Cambridge Structural Database.

Author contributions

J. Mai: conceptualization, investigation, validation, formal analysis, writing – original draft, visualization. B. Rösch: investigation, validation, formal analysis. N. Patel: investigation, validation, formal analysis. J. Langer: formal analysis, validation. Sjoerd Harder: conceptualization, writing – original draft – review and editing, visualization, validation, supervision, project administration.

Conflicts of interest

There are no conflicts to declare.

Acknowledgements

We acknowledge Mrs A. Roth (University of Erlangen-Nürnberg) for CHN analyses and J. Schmidt and Dr C. Färber (University of Erlangen-Nürnberg) for assistance with the NMR analyses. We acknowledge the Deutsche Forschungsgemeinschaft (DFG) for funding this project (HA 3218/11-1). Dr Neha Patel is grateful for funding from the European Union's Horizon 2020 research and innovation programme as a Marie Skłodowska-Curie post-doctoral fellow on the NITRO-EARTH project (101064276).

References

1 S. P. Green, C. Jones and A. Stasch, *Science*, 2007, **318**, 1754–1757.
2 S. Krieck, L. Yu, M. Reiher and M. Westerhausen, *Eur. J. Inorg. Chem.*, 2010, 197–216.
3 A. Stasch and C. Jones, *Dalton Trans.*, 2011, **40**, 5659–5672.
4 C. Jones, *Nat. Rev. Chem.*, 2017, **1**, 0059.
5 L. A. Freeman, J. E. Walley and R. J. Gilliard Jr, *Nat. Synth.*, 2022, **1**, 439–448.
6 S. Krieck, H. Görls, L. Yu, M. Reiher and M. Westerhausen, *J. Am. Chem. Soc.*, 2009, **131**, 2977–2985.
7 M. Arrowsmith, H. Braunschweig, M. A. Celik, T. Dellermann, R. D. Dewhurst, W. C. Ewing, K. Hammond, T. Kramer, I. Krummenacher, J. Mies, K. Radacki and J. K. Schuster, *Nat. Chem.*, 2016, **8**, 890–894.
8 G. Wang, J. E. Walley, D. A. Dickie, S. Pan, G. Frenking and R. J. Gilliard, *J. Am. Chem. Soc.*, 2020, **142**, 4560–4564.
9 W. Huang and P. L. Diaconescu, *Dalton Trans.*, 2015, **44**, 15360–15371.
10 D. Jędrzkiewicz, J. Mai, J. Langer, Z. Mathe, N. Patel, S. DeBeer and S. Harder, *Angew. Chem., Int. Ed.*, 2022, **61**, e202200511.
11 M. Gimferrer, S. Danes, E. Vos, C. B. Yildiz, I. Corral, A. Jana, P. Salvador and D. M. Andrada, *Chem. Sci.*, 2022, **13**, 6583–6591.
12 S. Pan and G. Frenking, *Chem. Sci.*, 2023, **14**, 379–383.
13 M. Gimferrer, S. Danes, E. Vos, C. B. Yildiz, I. Corral, A. Jana, P. Salvador and D. M. Andrada, *Chem. Sci.*, 2023, **14**, 384–392.
14 S. J. Bonyhady, C. Jones, S. Nembenna, A. Stasch, A. J. Edwards and G. J. McIntyre, *Chem.–Eur. J.*, 2010, **16**, 938–955.
15 B. Rösch, T. X. Gentner, J. Langer, C. Färber, J. Eyselein, L. Zhao, C. Ding, G. Frenking and S. Harder, *Science*, 2021, **371**, 1125–1128.
16 B. Maitland, A. Stasch and C. Jones, *Aust. J. Chem.*, 2022, **75**, 543–548.
17 R. Mondal, K. Yuvaraj, T. Rajeshkumar, L. Maron and C. Jones, *Chem. Commun.*, 2022, **58**, 12665–12668.
18 Y. Liu, K. Zhu, L. Chen, S. Liu and W. Ren, *Inorg. Chem.*, 2022, **61**, 20373–20384.
19 T. X. Gentner, B. Rösch, G. Ballmann, J. Langer, H. Elsen and S. Harder, *Angew. Chem., Int. Ed.*, 2019, **58**, 607–611.
20 J. Mai, M. Morasch, D. Jędrzkiewicz, J. Langer, B. Rösch and S. Harder, *Angew. Chem., Int. Ed.*, 2023, **62**, e202212463.
21 B. Rösch, T. X. Gentner, J. Eyselein, J. Langer, H. Elsen and S. Harder, *Nature*, 2021, **592**, 717–721.
22 L. R. Murphy, T. L. Meek, A. L. Allred and L. C. Allen, *J. Phys. Chem. A*, 2000, **104**, 5867–5871.
23 T. Clark, *J. Am. Chem. Soc.*, 1988, **110**, 1672–1678.
24 P. Banerjee and P. K. Nandi, *Phys. Chem. Chem. Phys.*, 2016, **18**, 12505–12520.
25 S. P. Green, C. Jones and A. Stasch, *Angew. Chem., Int. Ed.*, 2008, **47**, 9079–9083.
26 B. Rösch, T. X. Gentner, J. Eyselein, A. Friedrich, J. Langer and S. Harder, *Chem. Commun.*, 2020, **56**, 11402–11405.
27 J. A. Platts, J. Overgaard, C. Jones, B. B. Iversen and A. Stasch, *J. Phys. Chem. A*, 2011, **115**, 194–200.
28 J. Overgaard, C. Jones, A. Stasch and B. B. Iversen, *J. Am. Chem. Soc.*, 2009, **131**, 4208–4209.
29 I. R. Speight, S. C. Chmely, T. P. Hanusa and A. L. Rheingold, *Chem. Commun.*, 2019, **55**, 2202–2205.
30 D. Jędrzkiewicz, J. Langer and S. Harder, *Z. Anorg. Allg. Chem.*, 2022, **648**, e202200138.
31 D. D. L. Jones, I. Douair, L. Maron and C. Jones, *Angew. Chem., Int. Ed.*, 2021, **60**, 7087–7092.
32 M. Garçon, A. J. P. White and M. R. Crimmin, *Chem. Commun.*, 2018, **54**, 12326–12328.
33 J. Pahl, S. Brand, H. Elsen and S. Harder, *Chem. Commun.*, 2018, **54**, 8685–8688.
34 L. Garcia, M. D. Anker, M. F. Mahon, L. Maron and M. S. Hill, *Dalton Trans.*, 2018, **47**, 12684–12693.

35 J. Pahl, A. Friedrich, H. Elsen and S. Harder, *Organometallics*, 2018, **37**, 2901–2909.
36 K. Thum, J. Martin, H. Elsen, J. Eyselein, L. Stiegler, J. Langer and S. Harder, *Eur. J. Inorg. Chem.*, 2021, 2643–2653.
37 K. Thum, A. Friedrich, J. Pahl, H. Elsen, J. Langer and S. Harder, *Chem.–Eur. J.*, 2021, **27**, 2513–2522.
38 L. M. Engelhardt, S. Harvey, C. L. Raston and A. H. White, *J. Organomet. Chem.*, 1988, **341**, 39–51.
39 C. Jones, L. McDyre, D. M. Murphy and A. Stasch, *Chem. Commun.*, 2010, **46**, 1511–1513.
40 J. J. Brooks, W. Rhine and G. D. Stucky, *J. Am. Chem. Soc.*, 1972, **94**, 7346–7351.
41 T. X. Gentner, B. Rösch, K. Thum, J. Langer, G. Ballmann, J. Pahl, W. A. Donaubauer, F. Hampel and S. Harder, *Organometallics*, 2019, **38**, 2485–2493.